frontiers | Frontiers in Nanotechnology

TYPE Original Research
PUBLISHED 11 August 2022
DOI 10.3389/fnano.2022.900379

Check for updates

OPEN ACCESS

EDITED BY
Manoj Saxena,
University of Delhi, India

REVIEWED BY
Asif Khan,
Georgia Institute of Technology, United States
Ashok Kumar,
National Physical Laboratory (CSIR), India

*CORRESPONDENCE
Maximilian Lederer,
maximilian.lederer@ipms.fraunhofer.de

SPECIALTY SECTION
This article was submitted to Nanoelectronics, a section of the journal Frontiers in Nanotechnology

RECEIVED 20 March 2022
ACCEPTED 19 July 2022
PUBLISHED 11 August 2022

CITATION
Lederer M, Seidel K, Olivo R, Kämpfe T and Eng LM (2022), Effect of Al_2O_3 interlayers on the microstructure and electrical response of ferroelectric doped HfO_2 thin films. *Front. Nanotechnol.* 4:900379. doi: 10.3389/fnano.2022.900379

COPYRIGHT
© 2022 Lederer, Seidel, Olivo, Kämpfe and Eng. This is an open-access article distributed under the terms of the Creative Commons Attribution License (CC BY). The use, distribution or reproduction in other forums is permitted, provided the original author(s) and the copyright owner(s) are credited and that the original publication in this journal is cited, in accordance with accepted academic practice. No use, distribution or reproduction is permitted which does not comply with these terms.

Effect of Al_2O_3 interlayers on the microstructure and electrical response of ferroelectric doped HfO_2 thin films

Maximilian Lederer[1]*, Konrad Seidel[1], Ricardo Olivo[1], Thomas Kämpfe[1] and Lukas M. Eng[2]

[1]Fraunhofer IPMS, Center Nanoelectronic Technologies, Dresden, Germany, [2]TU Dresden, Institut für Angewandte Physik, Dresden, Germany

Novel devices based on ferroelectric hafnium oxide comply with the increasing demand for highly scalable embedded non-volatile memory devices, especially for in-memory computing applications. However, due to the polycrystalline nature of these hafnium oxide films, highly scaled devices face variability concerns. In order to enable smaller grains to circumvent the current limitations, the introduction of Al_2O_3 interlayers to interrupt the columnar grain growth is presented herein. Transmission Kikuchi diffraction is utilized to investigate influences of the Al_2O_3 layer on the microstructure of hafnium oxide. Moreover, electrical analysis indicates how the interlayer affects the wake-up phenomena as well as the electric field distribution within the stack. These results provide evidence on how to control grain size, electric behavior, and crystallization temperature by the insertion of Al_2O_3 interlayers.

KEYWORDS

ferroelectric, hafnium oxide, heterostructure, transmission Kikuchi diffraction, X-ray diffraction

1 Introduction

The increasing demand for in-memory computing has led to renewed interests in embedded non-volatile memories. Especially ferroelectric field-effect transistors (FeFETs) have been suggested to enable fast and low power in-memory computing, reaching 13,714 TOPS/W. Soliman et al. (2020) These FeFETs have been realized by ferroelectric hafnium oxide, which is compatible with complementary-semiconductor-insulator-metal (CMOS) processes since it is already present in conventional high-k-metal-gate (HKMG) technology nodes. Due to their high coercive field and remanent polarization as well as the absence on dead layer effects, FeFETs can be realized with very thin hafnium oxide layer thicknesses, even below 10 nm Müller et al. (2015). As a result, such devices have already been demonstrated in highly scaled devices of the 22 and 28 nm technology Dünkel et al. (2017); Müller et al. (2012b) as well as in FinFET structures in even smaller technology nodes Krivokapic et al. (2017); De et al. (2021a).

Nevertheless, recent results have raised concerns regarding device-to-device variability due to the polycrystalline nature of the hafnium oxide layer Lederer et al. (2020); De et al. (2021b); Khan et al. (2020); Ni et al. (2020). In addition, front-end-of-line (FEoL) integrated FeFETs, where the ferroelectric layer is directly mounted on top of the channel separated from each other by a thin interface layer only, current percolation path effects have been reported to be present as well Müller et al. (2021); Lederer et al. (2021d). Consequently, methods to achieve smaller grains are crucial for improving device scaling.

Moreover, due to the metastable nature of the ferroelectric orthorhombic ($Pca2_1$) phase in hafnium oxide Materlik et al. (2015); Huan et al. (2014), polymorphism will additionally affect the variability. Other phases like e.g. the monoclinic phase that is resembling the ground state, will act as leakage path in the off-state and will generally increase variability in the drain current and switching behavior Kao et al. (2018). Finally, the crystallographic orientation of the polarization axis within each grain affects the switching behavior as well as the device variability Müller et al. (2021); Lederer et al. (2021d). Crystallographic analysis *via* transmission Kikuchi diffraction (TKD) Keller R. R. and Geiss (2012); Lederer et al. (2019) of hafnium oxide films have revealed the presence of strong crystallographic textures in the film Lederer et al. (2019, 2020). Under certain conditions, even semi-epitaxial growth was observed in polycrystalline layers Lombardo et al. (2021); Lederer et al. (2021b). It is therefore pivotal to consider crystallographic textures in the ferroelectric layer as well.

Here, the introduction of Al_2O_3 interlayers is explored in order to interrupt columnar grain growth and control the grain size. In contrast to previous research Kim et al. (2014); Riedel et al. (2016), which explored the insertion of Al_2O_3 layers for stabilizing the ferroelectric phase in thicker HfO_2 layers (> 20 nm), this work focuses on achieving smaller grains in 10 nm films for improved device-to-device variability. Therefore, the crystallographic texture as well as the electrical behavior of these heterostructures is explored. For this, a novel analysis method called transmission Kikuchi diffraction (TKD) is utilized, which enables the analysis of the local crystallographic phases and orientation as well as the microstructure by collecting the Kikuchi diffraction patterns of scattered electrons at each scanning point using a scanning electron microscope Keller R. R. and Geiss (2012).

2 Materials and methods

The doped HfO_2-Al_2O_3 heterostructures were formed by atomic layer deposition (ALD) on an 10 nm thick TiN layer that was deposited *via* ALD on highly-doped silicon substrates. $HfCl_4$ and trimethylaluminium (TMA) were used as precursor for the HfO_2 and Al_2O_3 layers, respectively, with H_2O as oxidizer. For Si- and Zr- doping, $SiCl_4$ and $ZrCl_4$ were used, respectively. The Al_2O_3 layers were deposited with a thickness of 0.6 nm, whereas the thickness of the individual doped HfO_2 layers ranged from 2.5 to 10 nm. The thickness of all hafnium oxide layers in the heterostructure was kept at a total of 10 nm, except for the sample used in the TKD analysis (20 nm), since thicker layers were required for sufficient signal quality. Here, a Al_2O_3 layer was inserted after 10 nm. For better readability, the terms 2 × 5 nm and 3 × 3.3 nm were used for the 10 nm thick heterostructures to indicate the number of doped HfO_2 layers (with their respective thickness) separated by Al_2O_3 layers. Furthermore, the doping concentration is provided in terms of cycling ratio of Hf:Zr and Hf:Si during ALD, respectively. After forming the heterostructure, a capping TiN electrode with a thickness of 10 nm was manufactured on top using physical vapor deposition (PVD). Thereafter, rapid thermal annealing was performed at 800°C for Si:HfO_2 (HSO) and $Hf_{0.5}Zr_{0.5}O_2$ (HZO). For structural analysis additional samples were annealed at other temperatures.

For electrical analysis, Ti/Pt electrodes were sputtered on top using a shadow mask. Excess TiN between the contacts was removed *via* wet etching. An Aixacct TF3000 Analyzer is used for the polarization measurements. A frequency of 1 kHz is applied for the dynamic hysteresis measurement (DHM) as well as for the electric field cycling. The latter was performed at identical amplitude as the DHM.

For structural analysis, grazing-incident X-ray diffraction (GIXRD) is used. Here, the incident angle was set to 0.5°. For the TKD measurement, the dimpled sample was placed inside a scanning electron microscope and an acceleration voltage of 30 kV was used.

3 Results

Based on the deposition process, a layered structure as schematically shown in Figure 1A is formed. Due to the interlayers the microstructure of the individual layers should differ as compared to a single 10 nm film. As changes like grains size, crystallographic orientation, and phase might be present, the microstructure is investigated *via* GIXRD and TKD.

3.1 Structural analysis of HSO/HZO-Al_2O_3 heterostructures

The GIXRD pattern of the HZO heterostructures with a 1:1 cycling ratio annealed at 800°C (see Figure 1B) show a significant line broadening already after introducing the first Al_2O_3-interlayer. Such a broadening is usually related to a reduced grain size or microstress. The insertion of further interlayers leads to a reduction in signal intensity, resulting in fully amorphous HZO layers in case of the 4 × 2.5 nm structure. The applied annealing temperature is consequently not sufficient to crystallize the thinner layers, thus an increase in the

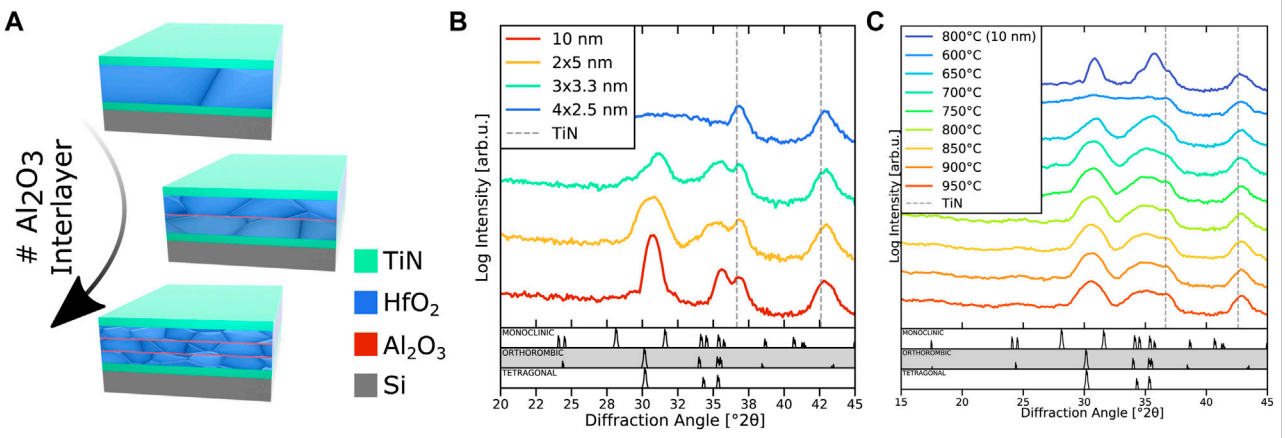

FIGURE 1
Structural analysis of doped HfO_2-Al_2O_3 heterostructures. **(A)** Schematic illustration of the heterostructure in dependence of the number of Al_2O_3 interlayers. GIXRD patterns for HZO/Al_2O_3 heterostructures are presented in **(B)**, showing a decrease of intensity of the diffraction line at 30°. The patterns collected for 2 × 5 nm HSO samples **(C)** indicate a crystallization between the annealing temperatures of 600 and 650°C. Wider diffraction lines are observed compared to the 10 nm HSO reference.

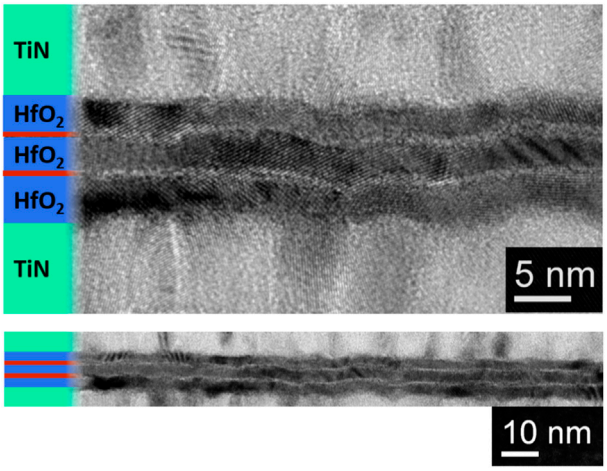

FIGURE 2
Transmission electron microscopy cross-section image of a 3 × 3.3 nm HfO_2/Al_2O_3 heterostructure after a 800°C anneal. Al_2O_3 layers appear as bright lines in between the HfO_2 layers, indicating no significant interdiffusion.

crystallization temperature can be concluded. Based on the position of the diffraction lines, it is obvious that no significant amount of monoclinic phase is present in the layers and the film consists predominately of orthorhombic/tetragonal phase.

In case of the GIXRD results (see Figure 1C) of the 2 × 5 nm HSO structure with a cycling ratio of 16:1, the crystallization temperature can be deduced to lie between 600 and 650°C, when comparing the patterns for different annealing temperatures. This crystallization temperature is about 100°C higher as compared to a 10 nm HSO film without interlayers, which lies around 550°C as reported previously Lederer et al. (2021b). Like the 2 × 5 nm film, broad diffraction lines are observable. Previously published GIXRD data of 10 nm HSO films without interlayer, showed similar line width as the 10 nm HZO film Lederer et al. (2020) and no significant change in the width of the diffraction lines has been reported for different annealing temperatures Lederer et al. (2021b). In comparison with these results it can therefore be concluded that, like in the case of HZO, smaller grains or increased microstress is expected in the 2 × 5 nm samples. Furthermore, no significant signal is observable for the lines with highest intensity of the monoclinic phase. Consequently, like in case of HZO, no significant portion of monoclinic phase is expected inside the layer.

Transmission electron microscopy images (see Figure 2) taken from the cross-section of a 3 × 3.3 nm HfO_2 stack reveal that the very thin (0.6 nm) Al_2O_3 interlayer do not interdiffuse into the adjacent layers but remain stable even after annealing at 800°C. Furthermore, it can be clearly observed that the crystal growth process is interrupted by these layers, since the orientation of the crystallites differ in vertical direction.

Since it has been reported previously, that crystallographic textures in hafnium oxide differ depending on the adjacent layers Lederer et al. (2021b, f) TKD analysis was performed on a HZO-Al_2O_3 heterostructure. As shown in Figure 3A, the quality map, which resembles the band contrast at each measurement point, visualizes a microstructure consisting of small disc shaped grains. However, in some regions (black regions), the signal quality is quite low and no individual grains can be distinguished. Possible

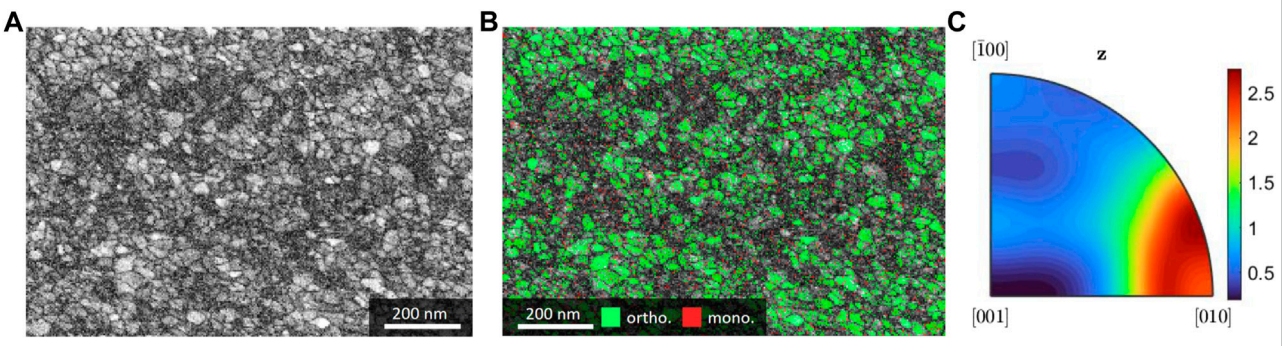

FIGURE 3
TKD analysis of a HZO/Al_2O_3 heterostructure. The grain structure can be observed in the quality map **(A)**, which visualized the measured band contrast. Phase extraction **(B)** indicates predominant orthorhombic phase. Crystallographic orientation is summarized by the inverse pole figure (IPF) in out-of-plane (z) direction **(C)**, indicating a pronounced texture of the [010]-axes aligning out-of-plane.

origins are either very fine grains or thickness variations, which result in a worse signal due to the interference of the second HZO layer. Interference from the Al_2O_3 layer is not expected due to its low thickness and amorphous nature.

By fitting simulated Kikuchi patterns of different crystallographic phases to the measured Kikuchi patterns, the present crystallographic phase can be inferred and a so-called phase map can be constructed. From the phase map shown in Figure 3 (here overlayed with the quality map), it can be observed that the majority of the grains is present in the orthorhombic phase. Due to the low signal quality in the aforementioned black regions, the phase could not be identified in these areas.

In addition, TKD allows to obtain information about the local crystallographic orientation Keller R. R. and Geiss (2012); Lederer et al. (2019). Figure 3C shows the inverse pole figure (IPF) of the film, which contains the orientation density of crystallographic axes along the out-of-plane direction. As can be observed here, a pronounced texture is present in the film. Most [010]-axes are pointing in out-of-plane direction, whereas the [001]-axes appear to be oriented in-plane. Since the [001]-axis resembles the polarization axis in the $Pca2_1$ phase, this would suggest very low polarization values to be measured. However, recent investigations strongly suggest that during the wake-up cycling of ferroelectric HfO_2 films a reorientation of the [010]- and [001]-axes takes place, mediated by 90°-domain wall movement (ferroelastic switching) Lederer et al. (2021e). Consequently, this crystallographic texture agrees with previously published data of HZO and HSO films with TiN bottom and top electrode Lederer et al. (2020). Since no significant differences in texture and grain size are observable, it can be concluded that the Al_2O_3 does not have a significant different influence on the microstructure compared to TiN for films of identical thickness. However, by keeping the total thickness constant when inserting interlayers, the grain size is expected to decrease based on GIXRD data. In addition, changes in the phase composition might occur and tetragonal or cubic phase might be present in ultra thin HfO_2 layers.

3.2 Impact of Zr content on the electrical behavior

Comparing now the results of the dynamic hysteresis measurements of the HZO films annealed at 800°C (see Figure 4), it can be observed that the remanent and saturated polarization ($2P_R$ and $2P_S$, respectively) reduce for the 1:1 cycling ratio with increasing amount of interlayers. However, after 10^4 electric field cycles all of the measured 10 nm devices without an Al_2O_3 interlayer had a breakdown. With one interlayer, a few devices survived and for the 3 × 3.3 nm devices no breakdown was observed. Consequently, the introduction of Al_2O_3 appears to lead to an increased endurance of the devices.

In addition, the dependence on the Zr concentration was investigated. For the 2 × 5 nm stack, an optimum concentration close to the 1:1 cycling ratio can be observed, both in $2P_R$ and $2P_S$. The decrease in $2P_S$ for high Zr content (Hf:Zr cycling ratio of 2:8 and 3:7) appears to be caused by very strong antiferroelectric-like behavior initially, as shown in Figure 4C and by the comparably low $2P_R$ values. This is also confirmed by the recovery after cycling. For low Zr concentrations, however, no antiferroelectric-like contributions are observed and the reduction is expected to be caused by the presence of monoclinic phase, like reported earlier for the doping dependence of HZO layers Müller et al. (2012a). Furthermore, the endurance is affected by the Zr content. For low concentrations, all devices show early breakdown, whereas higher concentrations lead to a stable operation.

For the 3 × 3.3 nm samples a shift in this concentration optimum is observable. Here the optimum lies close to the 7:3 Hf:Zr cycling ratio

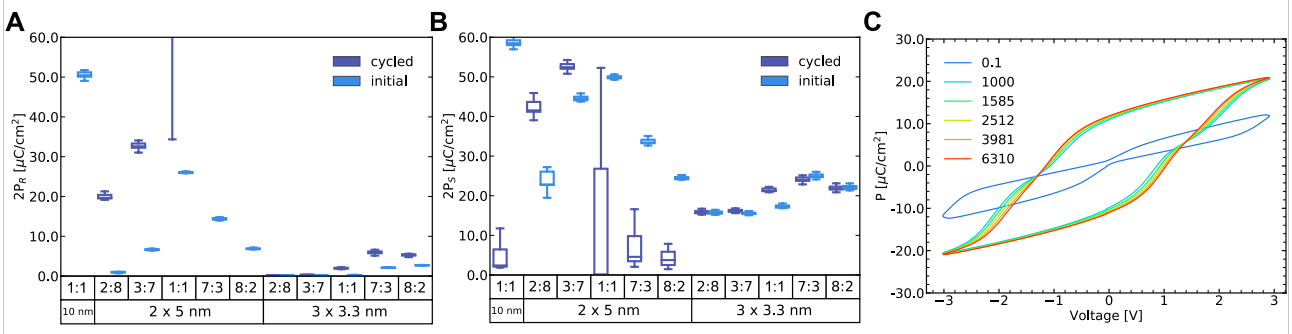

FIGURE 4
Electrical analysis of HZO/Al_2O_3 heterostructures with varying Zr content. **(A,B)** visualize the remanent (2 PR) and saturated (2 PS) polarization of the pristine and cycled device for 3 V cycling and DHM amplitude, respectively. 2PS values close to zero indicate breakdown. Strong antiferroelectric-like behavior is observed in the polarization-voltage hysteresis of the 2 × 5 nm HZO sample with a cycling ratio of Hf:Zr 3:7 **(C)**. The number of applied electric stress cycles is provided in the legend.

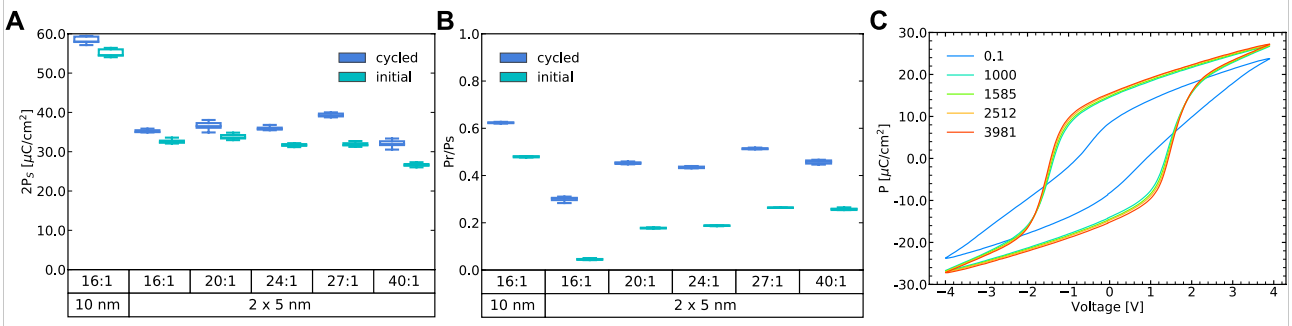

FIGURE 5
HSO-based heterostructure performance based on electrical measurements. 2PS results and the PR/PS ratio of the pristine and cycled device are given in **(A,B)**, respectively, for an cycling and DHM amplitude of 3 V. No strong impact on 2 PS is observed in dependence on the cycling ratio. **(C)** Visualized the polarization-voltage hysteresis over electric field cycling for the 2 × 5 nm HSO sample with a cycling ratio of 27:1. Here an increased cycling and DHM amplitude of 4 V is used. The number of applied electric cycles is provided in the legend.

based on the $2P_S$ data. Moreover, no early breakdown is observed in all devices. Due to the shift in the optimal concentration it can be furthermore observed that the samples with very high Zr content do not show significant amounts of $2P_R$ and $2P_S$. They therefore appear to behave almost dielectric.

3.3 Si-doped HfO_2-Al_2O_3 heterostructures

In case of Si doping a reduction in $2P_R$ and $2P_S$ is observable as well when introducing an interlayer (see Figure 5). This reduction can be counteracted applying higher voltages, as shown in Figure 5C, indicating that the parasitic capacitance introduced by the Al_2O_3-layer acts as a voltage divider. In contrast to the HZO layers the doping dependence appears to be different. While an optimum is clearly present in the $2P_S$ results for HZO, the $2P_S$ values of the 2 × 5 nm HSO layers are all around the same level and only a small drop can be observed for the lowest cycling ratio (Hf:Si 40:1). On the other hand, the initial P_R/P_S ratio shows a clear trend. With increasing Si content (from 40:1 to 16:1 Hf:Si cycling ratio) a reduction is observable, here. This indicates an increased antiferroelectric-like behavior. Compared to results on 10 nm HSO layers without interlayer, which reported a narrow doping window (showing a clear $2P_S$ optimum around 14:1 to 16:1 cycling ratio) Lederer et al. (2021c), a wider doping window can be concluded.

Another difference to the HZO samples is the increased endurance. While many HZO samples showed early breakdown in case of the 10 nm and 2 × 5 nm samples, no breakdown is observed in any of the HSO devices.

4 Discussion

From the above presented results it can be clearly observed that the optimum doping concentration of Zr and Si is shifting to lower concentrations when introducing the Al_2O_3 layers. This behavior is very similar to the thickness dependence of phase stabilization in undoped HfO_2 layers Polakowski and Müller (2015) as well as in HSO layers, where a shift in doping concentration to lower values was observed with decreasing thickness Yurchuk et al. (2013); Ali et al. (2019). The physical origin has been suggested to be related to residual stress due to thermal expansion coefficient mismatch Lederer et al. (2021e,a,b); Lederer et al. (2021e,a,b); Lederer et al. (2021e,a,b); Schenk et al. (2019). Since increasing antiferroelectric-like behavior is observable with thinner layers and the TKD measurements revealed an [001] in-plane texture, it fits very well with previously published results which provided evidence that the antiferroelectric-like behavior is related to 90°-domain wall movement Lederer et al. (2021e). As 90°domain wall movement is affected by mechanical stress due to its ferroelastic behavior, increased tensile in-plane stress due to the thinner layer will consequently lead to increased antiferroelectric-like behavior Lederer et al. (2021e); Ali et al. (2022); Lederer et al. (2021c); Kirbach et al. (2021). An important finding here is that these effects are also present in HZO layers, as indicated by the shift in the optimum doping concentration, thus providing evidence that these mechanisms are applicable for the HfO_2/ZrO_2 material system in general.

Based on the TKD results it can furthermore be concluded that the interface to an Al_2O_3 interlayer does not have a significant impact on the grain growth inside individual layers, as no major difference to crystallographic textures and grain shapes present in classical metal-ferroelectric-metal structures with two TiN interfaces is observed. This stands in high contrast to e.g. SiO_2-substrates which have been reported to strongly alter the growth process, resulting in larger grains of dendritic shape and $<110>$ out-of-plane texture Lederer et al. (2021f,b); Lederer et al. (2021f,b).

The results from the GIXRD patterns, furthermore, confirm the expected decrease in grain size with increasing number of interlayers. This is explainable by the Al_2O_3-layers acting as growth barriers, interrupting the growth of columnar shaped grains. Consequently, more and smaller grains are present inside the heterostructure. This is of major advantage for highly scaled devices, e.g. for the application in neuromorphic circuits, since the device-to-device variability is reduced. This is especially important for front-end-of-line integrated FeFETs, since their switching behavior is governed by the presence of current percolation paths Müller et al. (2021). Moreover, nucleation limited switching Mulaosmanovic et al. (2017) suggests that the stabilization of high numbers of intragranular domains is expected to be challenging. Consequently, the access of intermediate states is strongly dependent on the number of grains inside highly-scaled FeFET devices.

In addition, the thinner layers and the suppressed growth result in an increased crystallization temperature, as confirmed by GIXRD as well. While this is of disadvantage for back-end-of-line integrated HfO_2-based devices, it is advantageous for front-end-of-line integrated FeFETs. As reported earlier, HZO-based FeFETs exhibit a larger memory window and better variability Lederer et al. (2020); Ali et al. (2019). However, due to the low crystallization temperature of HZO, these devices commonly suffer in terms of endurance due to degradation of the film quality after the high temperature dopant activation anneal in the CMOS process flow. As shown by the herein presented results, the HZO-Al_2O_3 heterostructures show improved endurance and increased crystallization temperatures, thus raising HZO to a suitable material candidate for front-end-of-line integrated FeFETs.

For HSO layers on the other hand, the introduction of these interlayers is not advantageous besides the reduction in grain size. Here, the disadvantage of parasitic capacitances due to the Al_2O_3 layer surpass the positive side effects of increased temperature stability. Nevertheless, the introduction of interlayers in HSO enables smaller grains and a wider doping process window. Especially the latter enables to precisely tune the degree of antiferroelectric-like behavior in this material.

5 Conclusion

In summary, the introduction of Al_2O_3 layers provide a framework to improve variability by controlling the grain size of the ferroelectric layer. Furthermore, the resulting increase in crystallization temperature enables improved endurance and makes HZO suitable for front-end-of-line applications. Structural analysis furthermore revealed that the Al_2O_3-layers, compared to TiN, do not significantly alter the crystal growth process equally thick layer, resulting in similar grain shapes and crystallographic textures. Moreover, the interlayers affect the optimal concentration of Zr or Si. Based on previously published works this has been related to a phase stabilization that is driven by mechanical stress.

Data availability statement

The original contributions presented in the study are included in the article/supplementary material, further inquiries can be directed to the corresponding author.

Author contributions

ML, TK, KS, and LE contributed to conception and design of the study. ML deposited and characterized the material. RO and ML performed the data analysis. ML wrote

the first draft of the manuscript. All authors contributed to manuscript revision, read, and approved the submitted version.

Funding

This research was funded by the ECSEL Joint Undertaking project TEMPO in collaboration with the European Union's Horizon 2020 Framework Program for Research and Innovation (H2020/2014-2020) and National Authorities, under Grant No. 826655, and by the German Bundesministerium für Wirtschaft (BMWi), by the State of Saxony in the frame of the Important Project of Common European Interest (IPCEI).

Conflict of interest

The authors declare that the research was conducted in the absence of any commercial or financial relationships that could be construed as a potential conflict of interest.

Publisher's note

All claims expressed in this article are solely those of the authors and do not necessarily represent those of their affiliated organizations, or those of the publisher, the editors and the reviewers. Any product that may be evaluated in this article, or claim that may be made by its manufacturer, is not guaranteed or endorsed by the publisher.

References

Ali, T., Lehninger, D., Lederer, M., Li, S., Kühnel, K., Mart, C., et al. (2022). Tuning hyrbrid ferroelectric and antiferroelectric stacks for low power FeFET and FeRAM applications by using laminated HSO and HZO films. *Adv. Electron. Mat.*, 2100837. doi:10.1002/aelm.202100837

Ali, T., Polakowski, P., Büttner, T., Kämpfe, T., Rudolph, M., Patzold, B., et al. (2019). "Principles and challenges for binary oxide based ferroelectric memory FeFET," in *IEEE international memory workshop* (Monterey, CA: IMW), 1–4. doi:10.1109/IMW.2019.8739651

De, S., Lu, D. D., Le, H.-H., Mazumder, S., Lee, Y.-J., Tseng, W.-C., et al. (2021a). "Ultra-low power robust 3bit/cell Hf0.5</inf>Zr0.5O2 ferroelectric FinFET with high endurance for advanced computing-in-memory technology," in *2021 symposium on VLSI technology*, 1–2.

De, S., Qiu, B.-H., Bu, W.-X., Baig, M. A., Sung, P.-J., Su, C.-J., et al. (2021b). Uniform crystal formation and electrical variability reduction in hafnium-oxide-based ferroelectric memory by thermal engineering. *ACS Appl. Electron. Mat.* 3, 619–628. doi:10.1021/acsaelm.0c00610

Dünkel, S., Trentzsch, M., Richter, R., Moll, P., Fuchs, C., Gehring, O., et al. (2017). A FeFET based super-low-power ultra-fast embedded NVM technology for 22nm FDSOI and beyond. In *IEEE international electron devices meeting*, 197. Piscataway, NJ: IEEE, 1–19.7.4. doi:10.1109/IEDM.2017.8268425

Huan, T. D., Sharma, V., Rossetti, G. A., and Ramprasad, R. (2014). Pathways towards ferroelectricity in hafnia. *Phys. Rev. B* 90, 064111. doi:10.1103/PhysRevB.90.064111

Kao, M.-Y., Sachid, A. B., Lin, Y.-K., Liao, Y.-H., Agarwal, H., Kushwaha, P., et al. (2018). Variation caused by spatial distribution of dielectric and ferroelectric grains in a negative capacitance field-effect transistor. *IEEE Trans. Electron Devices* 65, 4652–4658. doi:10.1109/TED.2018.2864971

Keller, R. R., and Geiss, R. H. (2012). Transmission EBSD from 10 nm domains in a scanning electron microscope. *J. Microsc.* 245, 245–251. doi:10.1111/j.1365-2818.2011.03566.x

Khan, A. I., Keshavarzi, A., and Datta, S. (2020). The future of ferroelectric field-effect transistor technology. *Nat. Electron.* 3, 588–597. doi:10.1038/s41928-020-00492-7

Kim, H. J., Park, M. H., Kim, Y. J., Lee, Y. H., Jeon, W., Gwon, T., et al. (2014). Grain size engineering for ferroelectric Hf 0.5 Zr 0.5 O 2 films by an insertion of Al 2 O 3 interlayer. *Appl. Phys. Lett.* 105, 192903. doi:10.1063/1.4902072

Kirbach, S., Lederer, M., Eßlinger, S., Mart, C., Czernohorsky, M., Weinreich, W., et al. (2021). Doping concentration dependent piezoelectric behavior of Si:HfO 2 thin-films. *Appl. Phys. Lett.* 118, 012904. doi:10.1063/5.0026990

Krivokapic, Z., Rana, U., Galatage, R., Razavieh, A., Aziz, A., Liu, J., et al. (2017). 14nm Ferroelectric FinFET technology with steep subthreshold slope for ultra low power applications. In *IEEE international electron devices meeting*, 15. Piscataway, NJ: IEEE 1.1–15.1.4. doi:10.1109/IEDM.2017.8268393

Lederer, M., Abdulazhanov, S., Olivo, R., Lehninger, D., Kämpfe, T., Seidel, K., et al. (2021a). Electric field-induced crystallization of ferroelectric hafnium zirconium oxide. *Sci. Rep.* 11, 22266. doi:10.1038/s41598-021-01724-2

Lederer, M., Bagul, P., Lehninger, D., Mertens, K., Reck, A., Olivo, R., et al. (2021b). Influence of annealing temperature on the structural and electrical properties of Si-doped ferroelectric hafnium oxide. *ACS Appl. Electron. Mat.* 3, 4115–4120. doi:10.1021/acsaelm.1c00590

Lederer, M., Kämpfe, T., Olivo, R., Lehninger, D., Mart, C., Kirbach, S., et al. (2019). Local crystallographic phase detection and texture mapping in ferroelectric Zr doped HfO2 films by transmission-EBSD. *Appl. Phys. Lett.* 115, 222902. doi:10.1063/1.5129318

Lederer, M., Kämpfe, T., Vogel, N., Utess, D., Volkmann, B., Ali, T., et al. (2020). Structural and electrical comparison of Si and Zr doped hafnium oxide thin films and integrated FeFETs utilizing transmission Kikuchi diffraction. *Nanomater. (Basel).* 10, 384. doi:10.3390/nano10020384

Lederer, M., Mertens, K., Olivo, R., Kühnel, K., Lehninger, D., Ali, T., et al. (2021c). Substrate-dependent differences in ferroelectric behavior and phase diagram of Si-doped hafnium oxide. *J. Mat. Res.* 36, 4370–4378. doi:10.1557/s43578-021-00415-y

Lederer, M., Müller, F., Varanasi, A., Olivo, R., Mertens, K., Lehninger, D., et al. (2021d). "Influence of microstructure on the variability and current percolation paths in ferroelectric hafnium oxide based neuromorphic FeFET synapses," in *2021 silicon Nanoelectronics workshop*, 1–2. doi:10.1109/SNW51795.2021.00033

Lederer, M., Olivo, R., Lehninger, D., Abdulazhanov, S., Kämpfe, T., Kirbach, S., et al. (2021e). On the origin of wake–up and antiferroelectric–like behavior in ferroelectric hafnium oxide. *Phys. Rapid Res. Ltrs.* 15, 2100086. doi:10.1002/pssr.202100086

Lederer, M., Reck, A., Mertens, K., Olivo, R., Bagul, P., Kia, A., et al. (2021f). Impact of the SiO 2 interface layer on the crystallographic texture of ferroelectric hafnium oxide. *Appl. Phys. Lett.* 118, 012901. doi:10.1063/5.0029635

Lombardo, S. F., Tian, M., Chae, K., Hur, J., Tasneem, N., Yu, S., et al. (2021). Local epitaxial-like templating effects and grain size distribution in atomic layer deposited Hf 0.5 Zr 0.5 O 2 thin film ferroelectric capacitors. *Appl. Phys. Lett.* 119, 092901. doi:10.1063/5.0057782

Materlik, R., Künneth, C., and Kersch, A. (2015). The origin of ferroelectricity in Hf1 – xZrxO2 : A computational investigation and a surface energy model. *J. Appl. Phys.* 117, 134109. doi:10.1063/1.4916707

Mulaosmanovic, H., Ocker, J., Müller, S., Schröder, U., Müller, J., Polakowski, P., et al. (2017). Switching kinetics in nanoscale hafnium oxide based ferroelectric field-effect transistors. *ACS Appl. Mat. Interfaces* 9, 3792–3798. doi:10.1021/acsami.6b13866

Müller, F., Lederer, M., Olivo, R., Ali, T., Hoffmann, R., Mulaosmanovic, H., et al. (2021). "Current percolation path impacting switching behavior of ferroelectric FETs," in *International symposium on VLSI technology, systems and applications (VLSI-TSA)*, 1–2. doi:10.1109/VLSI-TSA51926.2021.9440081*VLSI-TSA*

Müller, J., Böscke, T. S., Schröder, U., Müller, S., Bräuhaus, D., Böttger, U., et al. (2012a). Ferroelectricity in simple binary ZrO2 and HfO2. *Nano Lett.* 12, 4318–4323. doi:10.1021/nl302049k

Müller, J., Polakowski, P., Müller, S., and Mikolajick, T. (2015). Ferroelectric hafnium oxide based materials and devices: Assessment of current status and future prospects. *ECS J. Solid State Sci. Technol.* 4, N30–N35. doi:10.1149/2.0081505jss

Müller, J., Yurchuk, E., Schlosser, T., Paul, J., Hoffmann, R., Müller, S., et al. (2012b). "Ferroelectricity in HfO2 enables nonvolatile data storage in 28 nm HKMG," in *IEEE symposium on VLSI technology*. Editor I. Staff (Honolulu, HI: VLSI), 25–26. doi:10.1109/VLSIT.2012.6242443

Ni, K., Gupta, A., Prakash, O., Thomann, S., Hu, X. S., and Amrouch, H. (2020). "Impact of extrinsic variation sources on the device-to-device variation in ferroelectric FET," in *IEEE international reliability physics symposium* (Dallas, TX: IRPS), 1–5. doi:10.1109/IRPS45951.2020.9128323

Polakowski, P., and Müller, J. (2015). Ferroelectricity in undoped hafnium oxide. *Appl. Phys. Lett.* 106, 232905. doi:10.1063/1.4922272

Riedel, S., Polakowski, P., and Müller, J. (2016). A thermally robust and thickness independent ferroelectric phase in laminated hafnium zirconium oxide. *AIP Adv.* 6, 095123. doi:10.1063/1.4964300

Schenk, T., Fancher, C. M., Park, M. H., Richter, C., Künneth, C., Kersch, A., et al. (2019). On the origin of the large remanent polarization in La:HfO2. *Adv. Electron. Mat.* 5, 1900303. doi:10.1002/aelm.201900303

Soliman, T., Müller, F., Kirchner, T., Hoffmann, T., Ganem, H., Karimov, E., et al. (2020). Ultra-low power flexible precision FeFET based analog in-memory computing. In *IEEE international electron devices meeting*, 29, 2.1–29.2.4. doi:10.1109/IEDM13553.2020.9372124

Yurchuk, E., Müller, J., Knebel, S., Sundqvist, J., Graham, A. P., Melde, T., et al. (2013). Impact of layer thickness on the ferroelectric behaviour of silicon doped hafnium oxide thin films. *Thin Solid Films* 533, 88–92. doi:10.1016/j.tsf.2012.11.125